Supporting Information for:

Microfluidic Self-Assembly of Folate-Targeted Monomolecular siRNA-Lipid Nanoparticles.

Rafał Krzysztoń, [a, b, d] Bässem Salem,[a] Dian-Jang Lee,[c, d] Gerlinde Schwake,[a] Ernst Wagner,[c, d] Joachim O.Rädler* [a, b, d]*

[a] *Department of Physics, Ludwig-Maximilians-Universität Munich (LMU), Geschwister-Scholl-Platz 1, Munich 80539, Germany.*
[b] *Graduate School of Quantitative Biosciences (QBM), Ludwig-Maximilians-Universität Munich (LMU), Geschwister-Scholl-Platz 1, Munich 80539, Germany,*
[c] *Department of Pharmacy, Ludwig-Maximilians-Universität Munich (LMU), Butenandtstr. 5-13, Munich 81377, Germany.*
[d] *Center for NanoScience (CeNS) and Nanosystems Initiative Munich (NIM), Schellingstr. 4, 80799 Munich, Germany.*
* Corresponding authors: J.O. Rädler - raedler@lmu.de, R. Krzysztoń - r.krzyszton@physik.lmu.de

1. FCS analysis:

To determine correlation times and fractions of diffusing particles, two mathematical models were used. The model for single-component systems (e.g. dsDNA, dsDNA + lipids in 50 % (v/v) isopropanol/H_2O) uses one 3D diffusion and one triplet component:

$$G(\tau) = A_0 + \frac{1}{n}\frac{1}{(1+\tau/\tau_{diff})}\frac{1}{\sqrt{1+\tau/(SP^2\tau_{diff})}}\left(1+\frac{Te^{-\tau/\tau_{trip}}}{1-T}\right) \quad \text{(s1)}$$

where: A_0 – offset, n – effective number of particles in confocal volume, τ_{diff} – diffusion time (correlation time), SP- structural parameter, T – fraction of particles in triplet state, τ_{trip} – characteristic residence time in triplet state

In the case of lipid/DNA samples, residual, freely diffusing dsDNA molecules are also present in the system (see section 3 in Supplementary Data). Here, a model with two 3D diffusion components and one triplet component was used:

$$G(\tau) = A_0 + \frac{1}{n\left(F+\alpha(1-F)\right)^2}\left(1+\frac{Te^{-\tau/\tau_{trip}}}{1-T}\right)\left[\frac{1}{(1+\tau/\tau_1)}\frac{1}{\sqrt{1+\tau/(SP^2\tau_1)}}+\alpha^2\frac{1-F}{(1+\tau/\tau_2)}\frac{1}{\sqrt{1+\tau/(SP^2\tau_2)}}\right] \quad \text{(s2)}$$

where: A_0 – offset, n – effective number of particles in confocal volume ($n=n_1+n_2$), τ_1 – diffusion time (correlation time) of particle species 1, τ_2 – diffusion time (correlation time) of particle species 1, F – fraction of molecules of species 1 ($F = n_1/(n_1+n_2)$), α – relative molecular brightness of particles 1 and 2 ($\alpha = q_2/q_1$), *SP*- structural parameter, T – fraction of particles in triplet state, τ_{trip} – characteristic residence time in triplet state.

Diffusion times τ_2 and τ_{diff} are also denoted as τ_{DNA} as they correspond directly to the diffusion of free dsDNA. The diffusion time τ_1 is further denoted as τ or τ_{mNALP}.

The fraction of lipid/DNA and free DNA particles was determined directly by fitting. For optimal concentration conditions of mNALP preparation the relative brightness of particles (α) was fixed to 1. Under these conditions, the parameter F can be used to estimate the DNA encapsulation in mNALPs.

The concentration was determined as the number of diffusing particles (n) in relation to rhodamine 6G or Alexa488 reference.

Data analysis was done with PyCorrFit software, developed by Thomas Weidemann (Max Planck Institute of Biochemistry, Martinsried, Germany) and Paul Müller (Biotechnology Center of the TU Dresden, Germany)

2. Evaluation of starting conditions

Starting conditions for molecular solutions (in 50% (v/v) isopropanol/H_2O) prior to mNALP formation were assessed by using fluorescence correlation spectroscopy (FCS) to check that isopropanol prevents lipid/DNA aggregation without precipitating the DNA.

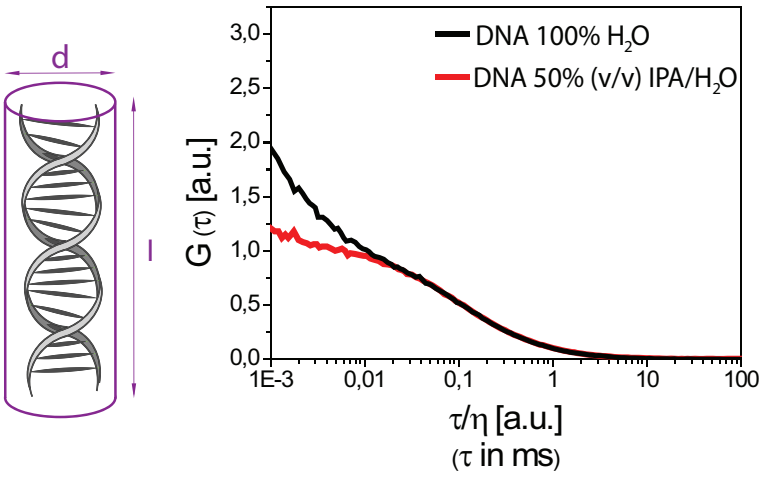

Figure S1. Cylindrical model of the 21-bp double-stranded DNA and viscosity-normalised FCS autocorrelation curves of naked DNA in 50 % (v/v) isopropanol/H_2O and pure H_2O. DNA concentration , c_{DNA} = 50 nM.

By applying the parameters of the B form of the DNA double helix, the theoretical values of diffusion coefficients for a 21-bp double-stranded DNA are calculated for both solvent conditions according to the modified Stokes-Einstein equation:

$$D = \frac{Ak_bT}{3\pi\eta l} \qquad \text{(s3)}$$

where: $A = ln(l/d) + 0.312 + 0.565*d/l - 0.1*d^2/l^2$; l – the length of the cylinder (Figure S1); d – the cylinder diameter (Figure S1); k_b – Boltzmann constant; η – solvent viscosity; T – temperature in degrees Kelvin. The experimental values of diffusion coefficients were obtained by taking the diffusion coefficient of rhodamine as reference (Table S1). The values are in good agreement, indicating that no precipitation of DNA occurs (Figure S2).

Table S1. Diffusion coefficients of naked 21-bp double-stranded DNA

Diffusion coefficients	Theoretical predictions (cylindrical model)	Experimental data
	D_{DNA} [cm^2 s^{-1}]	D_{DNA} [cm^2 s^{-1}]
H_2O	$9.02 \cdot 10^{-7}$	$(1.10 \pm 0.19) \cdot 10^{-6}$
50 % (v/v) isopropanol/H_2O	$2.5 \cdot 10^{-7}$	$(2.81 \pm 0.22) \cdot 10^{-7}$

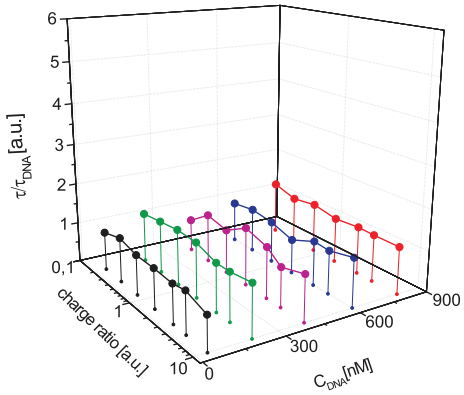

Figue S2. Relative diffusion time of DNA in the presence of lipids (DOTAP:DOPE:DOPC:DSPE-PEG(2000) in molar ratios 1:5:6:1.2 in 50% (v/v) isopropanol/H_2O) for different total DNA concentrations. Lipid concentration is expressed as the charge ratio of the cationic DOTAP to the polyanionic DNA. No significant change in relative diffusion times is seen.

The hydrodynamic radius of naked 21-bp dsDNA was calculated directly from the experimental diffusion coefficient and equals $R_h = 2.37$ nm. The hydrodynamic radius of loaded nanoparticles was calculated by multiplying relative diffusion times (τ/τ_{DNA}) by this value.

3. Microfluidic mixing at low Reynolds numbers

The solvent-exchange method is based on mixing of lipids or polymers dissolved in an organic solvent with an aqueous solution of nucleic acids (NAs). The change in solvent environment leads to a decrease in lipid/polymer solubility, and consequently to interaction

with NAs and self-assembly of complexes. The bottleneck in this approach is the lack of control over the mixing process when macroscopic mixing methods (*e.g.* vortexing) are used. Particle properties are sensitive to local mixing times.[1-3] In particular, long times may result in the dominance of mass transport, with formation of large particles of variable structure and composition. Macroscopic mixing is associated with a broad range of local mixing times and hence with spatial inhomogeneities in terms of supersaturation, nucleation and growth of particles. These effects lead to a broader size distribution of the product, variations in particle morphology and poor batch-to-batch reproducibility. However, by scaling down the process to the micrometer scale, one gains greater control over mixing kinetics, and undesirable or unintended effects can be minimized.[1-6] With the use of microfluidic techniques, the mixing time is reduced to milliseconds. In addition, flow on the micrometer length scale is characterized by low Reynolds numbers ($Re < 2000$) and is purely laminar. Thus micromixing occurs solely by diffusion and turbulent mass transport is minimized.

In a hydrodynamic focusing channel geometry, mixing occurs rapidly by diffusion due to the narrow width of the focused central flow. The mixing time can be estimated according to a two-dimensional model as described by Karnik et al.[1] Assuming that the Poiseuille flow profile in a channel of width w with pressure gradient dP/dx along its length is given by

$$u(y) = \frac{1}{8\mu}\frac{dP}{dx}(w^2 - 4y^2) \tag{s4}$$

where μ is the fluid viscosity,

and that the fluid profile is not significantly disrupted by the viscosity of the central alcohol stream, then the average velocity of the central stream can be approximated as

$$u_{f,avg} \approx u(0) = \frac{1}{8\mu}\frac{dP}{dx}w^2. \tag{s5}$$

Viscosity does not change the velocity of the central stream if the relation

$$\frac{w_f^2}{\mu_f} \ll \frac{w^2}{\mu} \tag{s6}$$

is satisfied. This condition holds for flow focussing of a 50% (v/v) isopropanol/water mixture ($\mu_f \sim 3.62$ cP) by two adjacent water flows ($\mu \sim 0.9$ cP) in the channel geometry used here. For a flow ratio *R* of central to adjacent streams, the width of the focused stream is given by

$$w_f \approx \frac{2w}{3(1+1/R)} \tag{s7}$$

Knowing that, the mixing time can be derived according to Fickian diffusion by the relation:

$$\tau_{mix} \sim \frac{w_f^2}{4D} \approx \frac{w^2}{9D} \frac{1}{(1+1/R)^2} \tag{s8}$$

In our chip design, the 200 μm wide outlet channel (*w*) results in a mixing time $\tau_{mix} \sim 34$ ms for a flow ratio *R* of 1/9 and assuming the isopropanol diffusivity $D \sim 10^{-9}$ m^2/s. However, this time corresponds to that taken for the change in solvent environment and does not take the dynamics of nanoparticle formation into account. To avoid possible negative effects of mass transport on particle formation, the outlet channel is extended to the length of 164 cm, allowing for full diffusive equilibration of the sample inside the channel. Furthermore, to minimize the diffusive distance between nucleic acids and lipids, all components were dissolved together in 50 % (v/v) isopropanol/water.

4. Microfluidic chip design:

The flow of liquids through the micro-sized channels is usually related to low Reynolds numbers (*Re*). Reynolds number is a measure of the importance of inertial in relation to viscous effects for given flow rate and length scale.

$$Re = \frac{\rho u L_h}{\mu} \tag{s9}$$

where: ρ – the density of the liquid, μ - liquid viscosity, L_h – the characteristic length scale of the system, *u* – average velocity of the liquid through the channel.

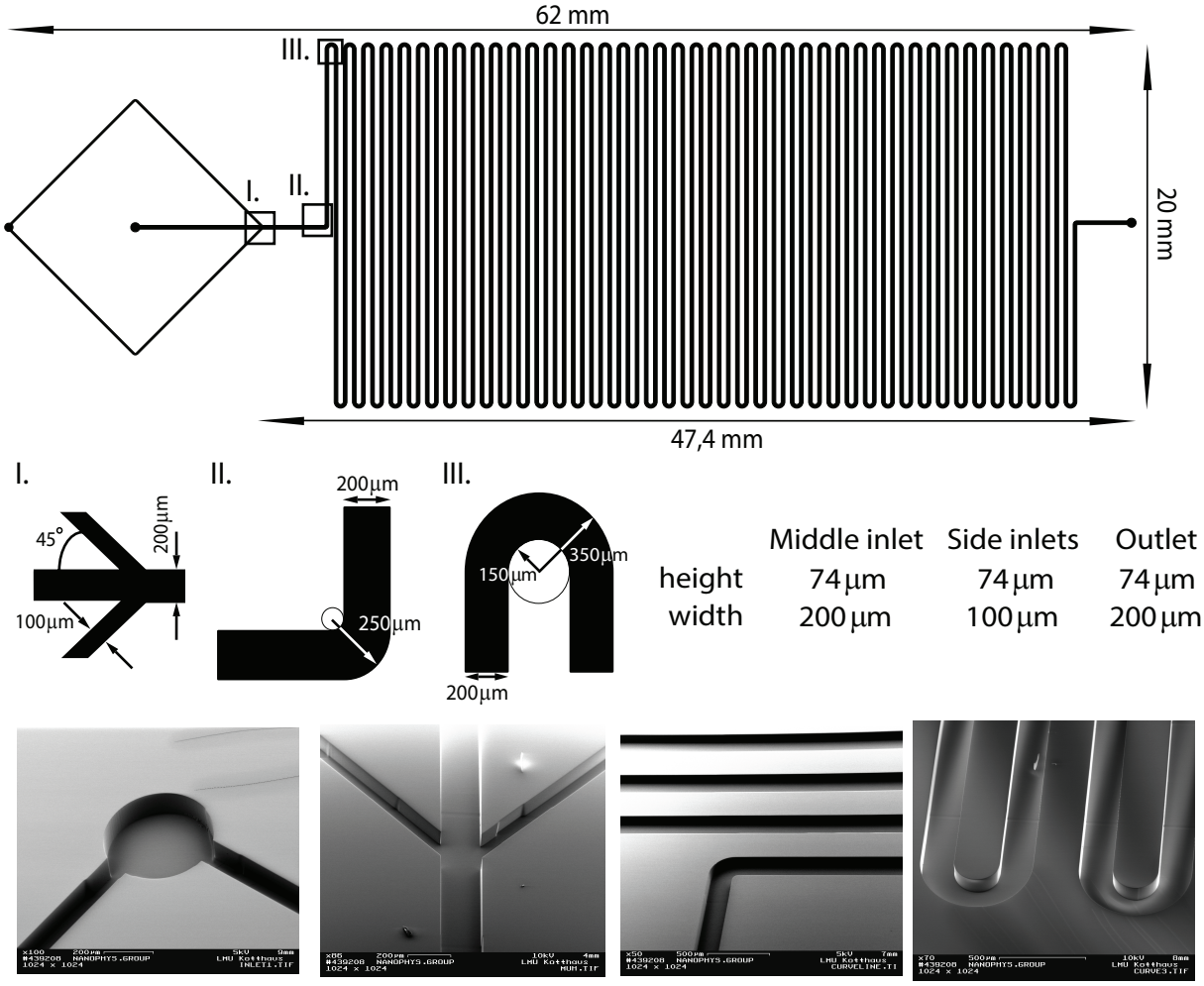

Figure S3. Microfluidic chip design and SEM images of PDMS channel. The inserts I, II, and III are showing the detailed view (and dimensions) of the fragments marked in the top overview image.

For our flow conditions, we assume the L_h to be equal to the channel width, w = 200 µm and the effects of different viscosity and density between 50 % (v/v) isopropanol/water and pure water flows ($\mu \sim 0.9$ cP, $\rho = 1$ g cm^{-3}) are negligible. Taking the total flow rate (Q) in the outlet channel of $Q = 1$ ml h^{-1} and given rectangular channel geometry (see **Figure.S3**), the average liquid velocity is in the range of $\boldsymbol{u \approx 0.019}$ **m s^{-1}** and the Reynolds number of $\boldsymbol{Re \approx 2}$. For the rectangular geometry systems described by low Reynolds numbers the relation between backpressure (ΔP) and the flow rate is given by equation **s10**.[7]

$$\Delta P = R_\Omega Q = \frac{a\mu QL}{wh^3} \qquad \text{(s10)}$$

$$a = 12\left[1 - \frac{192h}{\pi^5} tanh\left(\frac{\pi w}{2h}\right)\right] \quad \text{(s11)}$$

where: R_a – the flow resistance of the channel, μ - liquid viscosity, L – the length of the channel, h – height of the channel, w – width of the channel, Q – flow rate through the channel. For displacement driven flow with the rate of $\boldsymbol{Q}$ **= 1 ml h^{-1}**, flown inside the channel of height, $\boldsymbol{h}$ **= 74 μm**, width, $\boldsymbol{w}$ **= 200 μm** and length, $\boldsymbol{L}$ **= 164 cm** (channel flow resistance $\boldsymbol{R_a}$ **= 296.33*10^9 kg m^{-4} s^{-1}**) the backpressure equals $\boldsymbol{\Delta P}$ **= 822,91 mbar**.

Additionally, for curved channel the centrifugal inertia effects need to be taken into account. The relative importance of centrifugal forces in relation to viscous forces for those geometries is described by Dean number (*Dn*).

$$Dn = \sqrt{\frac{d}{2r}} Re \quad \text{(s12)}$$

where: r – the channel curvature radius, d – the hydraulic diameter of the channel. For rectangular channel cross section d is given by:

$$d = \frac{2hw}{h+w} \quad \text{(s13)}$$

In described geometry the first and last half turns ($\boldsymbol{r}$ **= 50 μm,** $\boldsymbol{d}$ **= 108 μm**) results in Dean numbers, $\boldsymbol{Dn}$ **= 2,11**. The full turns ($\boldsymbol{r}$ **= 150 μm,** $\boldsymbol{d}$ **= 108 μm**) results in $\boldsymbol{Dn}$ **= 1,22.**

In conclusion, the Reynolds number inside the outlet channel remains significantly below the critical values of transition (~1000) and turbulent flow regime (~2000) for selected flow rate. Also the Dean number in the curved parts of the channel remains below the critical value for first-order Dean vortex flow (~36).[8] Both, values of Reynolds and Dean numbers, suggest that the flow remain purely laminar. Observation of the flow in the T-junction position (Figure.1 in the main text) and up to ~90 mm downstream in the outlet channel (**Figure.S4**) promotes this finding as no signs of instabilities and other disruptions in laminar flow profile due to presence of alcohol and channel curvatures was seen.

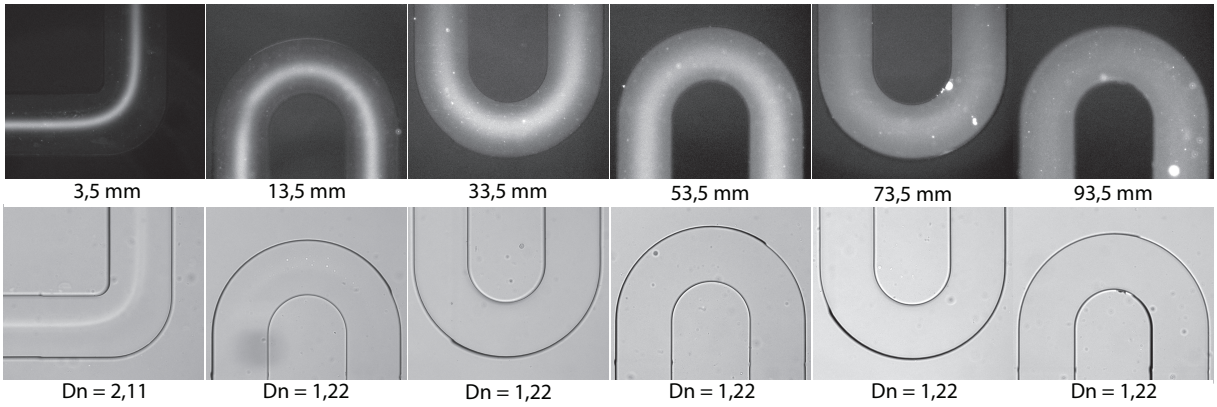

Figure S4. Bright-field and fluorescence micrographs of first 6 curved regions of meandering outlet channel. At the upstream T-junction two water streams from the side inlets squeeze the middle stream of 1 μM Cy3 in 50 % (v/v) isopropanol/H_2O resulting in narrow stream seen at the most left images (Total flow 1 mL h^{-1}; flow rate ratio 1:9). The downstream distance from the T-junction as well as the Dean numbers for given flow rate and geometry are given. The inertia effects are not disrupting the crossectional flow profiles in curved regions of the channel. The mixing occurs slowly within the channel due to Cy3 diffusion.

5. Assessment of mNALP assembly behavior

Deviations in residuals suggested that the two-component model is more suitable in this case (see **Figure S5**). The fraction of diffusing particles (*F*) was used as a direct measure of DNA encapsulation efficiency

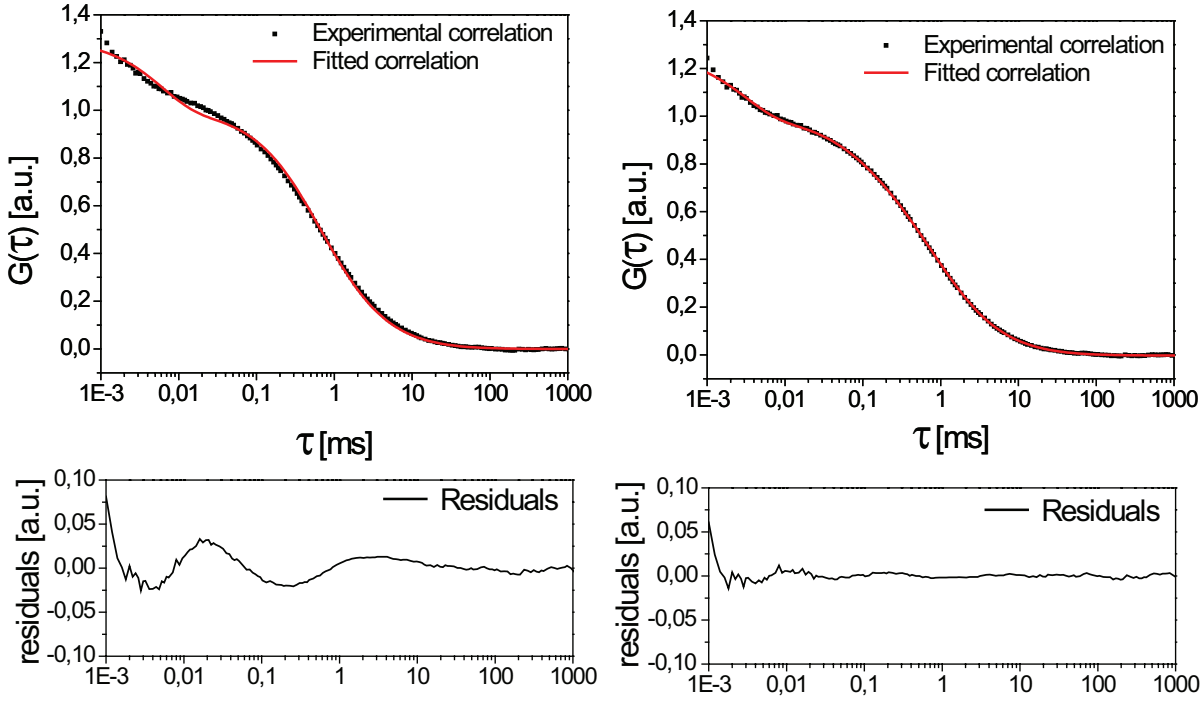

Figure S5. Comparison of one- (left) and two-component (right) correlation model fits to experimental data for mNALPs prepared by the bulk mixing method under optimal conditions (c_{DNA} = 40 nM, ρ = 5). The large deviation in the center of the residual plot for the one-component model was significantly reduced when the two-component model was used. The fast diffusion time obtained from the fit corresponds well with the times obtained for free 21-bp double stranded DNA.

5. FolA does not affect particle formation

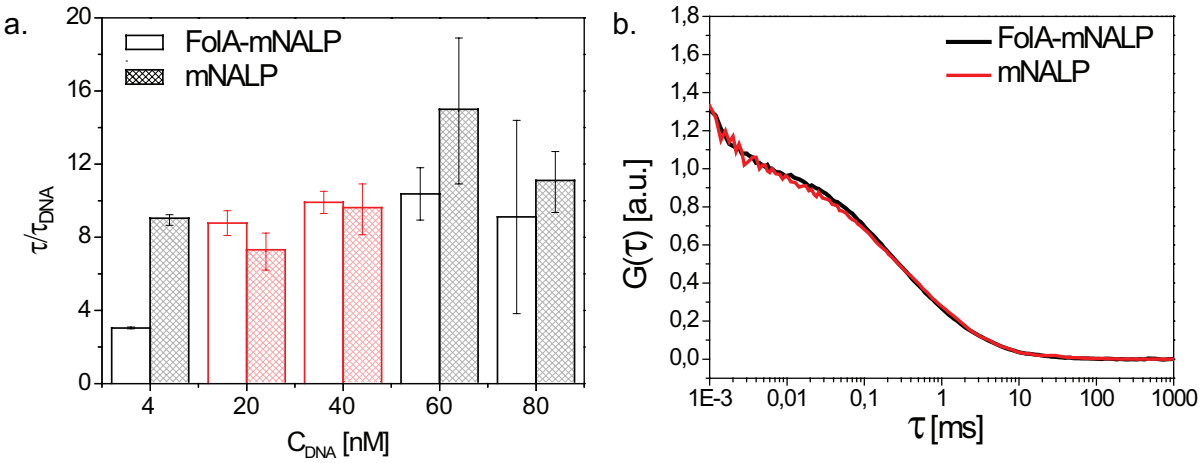

Figure S6. a. Comparison of relative diffusion times of targeted and non-targeted mNALPs formed at a charge ratio of ρ = 5. Data are plotted as a function of DNA duplex concentration. The samples were

prepared with the bulk mixing method. Optimal mNALP formation conditions are marked in red. b. Correlation curves obtained for FolA and non-FolA mNALPs prepared under optimal conditions c_{DNA} = 40 nM, ρ = 5. Curves show negligible deviation

6. mNALPs can be concentrated 35 fold

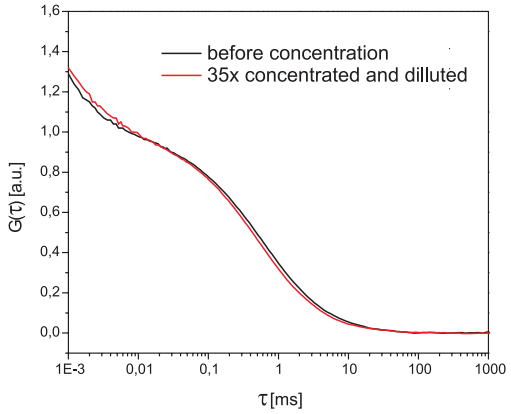

Figure S7. FCS correlation curves for FolA-mNALP prepared by the microfluidic mixing method under optimal conditions; c_{DNA} = 40 nM, ρ = 5 (black), and after 35x sample concentration (45 °C, high vacuum) and resuspension. Curves show negligible deviation, revealing the stability of the particles after concentration up to 1.4 μM.

7. FolA-mNALP stability in blood plasma and serum

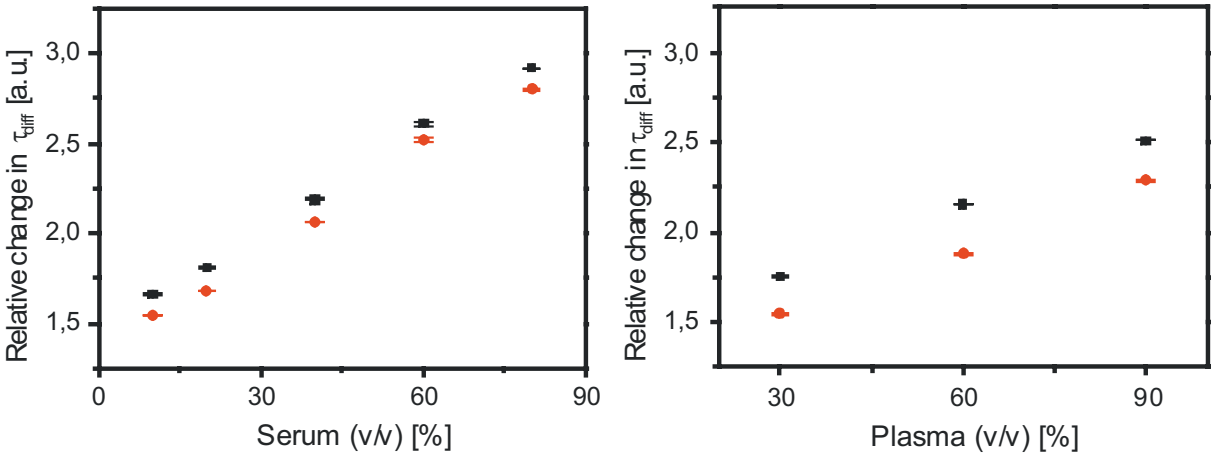

Figure S8. Similar linear changes in relative diffusion times of Cy3 (black) and Cy3-dsDNA (red) suggest that viscosity increase is the dominant factor in deviations between Cy3-dsDNA diffusion measured in serum and plasma. No degradation or unspecific protein binding was detected. Diffusion

times of Cy3 and Cy3-dsDNA in water are taken as a reference.

8. Folate receptor-mediated specific binding and uptake of FolA-mNALPs

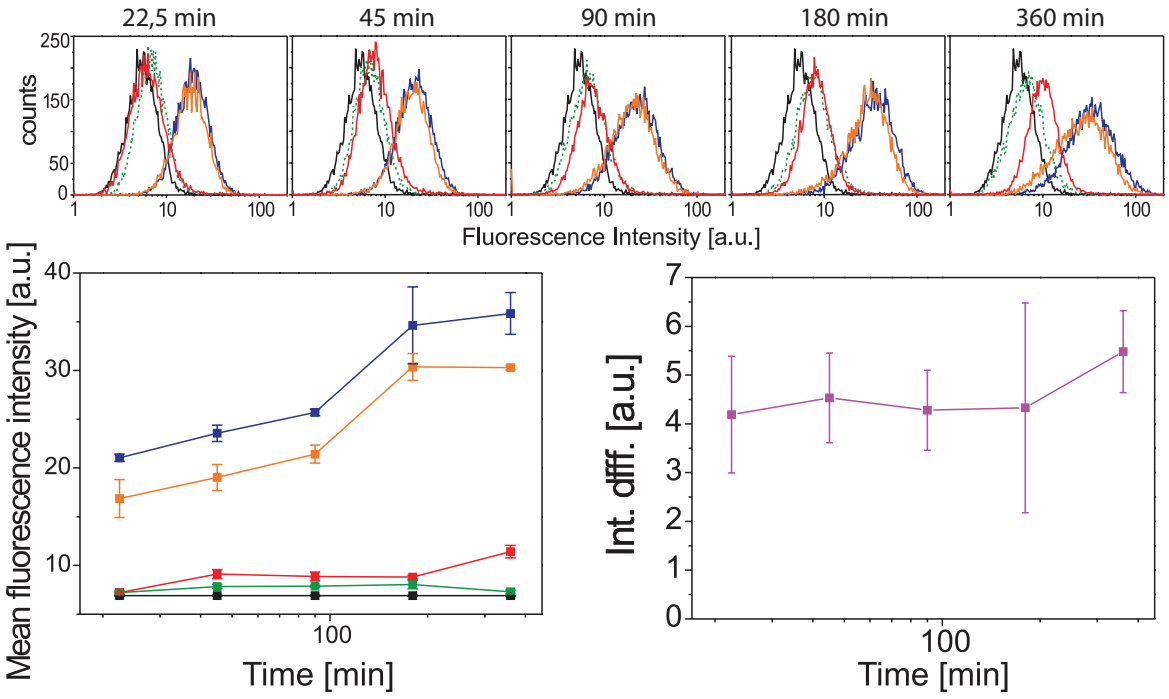

Figure S9. Time-course of specific binding and uptake of FolA-mNALPs into WT_KB cells overexpressing the folate receptor as determined by FACS. The purple trace shows the difference between mean fluorescence intensities of acid-treated and untreated cells, revealing the changes in the fraction of surface-bound mNALPs. Blue: FolA-mNALP containing ATTO488-dsDNA (receptor-bound and internalized fractions), orange: FolA-mNALP containing ATTO488-dsDNA (internalized fraction only) red: mNALP containing ATTO488-dsDNA, green: uncoated ATTO488-dsDNA, black: untreated cells).

References:

1 R. Karnik, F. Gu, P. Basto, C. Cannizzaro, L. Dean, W. Kyei-Manu, R. Langer and O. C. Farokhzad, *Nano Lett.*, 2008, **8**, 2906–12.

2 I. V. Zhigaltsev, N. Belliveau, I. Hafez, A. K. K. Leung, J. Huft, C. Hansen and P. R. Cullis, *Langmuir*, 2012, **28**, 3633–3640.

3 N. M. Belliveau, J. Huft, P. J. Lin, S. Chen, A. K. Leung, T. J. Leaver, A. W. Wild, J. B. Lee, R. J. Taylor, Y. K. Tam, C. L. Hansen and P. R. Cullis, *Mol. Ther. Nucleic Acids*, 2012, **1**, e37.

4 I. V Zhigaltsev, Y. K. Tam, A. K. K. Leung and P. R. Cullis, *J. Liposome Res.*, 2015, **2104**, 1–7.

5 A. Jahn, J. E. Reiner, W. N. Vreeland, D. L. DeVoe, L. E. Locascio and M. Gaitan, *J. Nanoparticle Res.*, 2008, **10**, 925–934.

6 A. K. K. Leung, I. M. Hafez, S. Baoukina, N. M. Belliveau, I. V. Zhigaltsev, E. Afshinmanesh, D. P. Tieleman, C. L. Hansen, M. J. Hope and P. R. Cullis, *J. Phys. Chem. C*, 2012, **116**, 18440–18450.

7 C. J. Morris and F. K. Forster, *Exp. Fluids*, 2004, **36**, 928–937.

8 J. D. Debus, M. Mendoza and H. J. Herrmann, *Phys. Rev. E - Stat. Nonlinear, Soft Matter Phys.*, 2014, **90**, 1–10.